IEEE Access
Multidisciplinary | Rapid Review | Open Access Journal

Received February 13, 2018, accepted March 16, 2018, date of publication March 21, 2018, date of current version May 16, 2018.

Digital Object Identifier 10.1109/ACCESS.2018.2817629

The Line Scan Camera Calibration Based on Space Rings Group

MENGHUI NIU[1,2], KECHEN SONG[1,2], XIN WEN[1,2], DEFU ZHANG[1,2], AND YUNHUI YAN[1,2]

[1]School of Mechanical Engineering and Automation, Northeastern University, Shenyang 110819, China
[2]Key Laboratory of Vibration and Control of Aero-Propulsion Systems Ministry of Education of China, Northeastern University, Shenyang 110819, China

Corresponding author: Kechen Song (songkc@me.neu.edu.cn)

This work was supported in part by the National Key Research and Development Program of China under Grant 2017YFB0304200, in part by the National Natural Science Foundation of China under Grant 51374063, and in part by the Fundamental Research Funds for the Central Universities under Grant N150308001.

ABSTRACT In addition to the accuracy requirements, the calibration of the line scan camera (LSC) should also have strong operability and portability. This paper presents a low-cost high-reliability LSC calibration method. First, a 3D right-angle stereo target based on concentric rings is designed, which is named space rings group, and it is suitable for static calibration of LSC. The calibration target has a simple structure and is easy to carry. The calibration process does not require other auxiliary instruments, greatly improving the operability of the calibration for the line camera. Second, in order to improve the positioning accuracy of subpixel edges in the image and reduce the computational complexity, a subpixel edge detection method is adopted, which is a region-by-region localization algorithm, a combination of global adaptive Canny detection and local partial area effect (Local-Canny-PAE, LCPAE). Then, the relationship between the actual spatial point and the image point is established by using the invariant nature of the image and the imaging model of the camera, and the two-step particle swarm optimization (TS_PSO) algorithm is used to solve the internal parameters of the camera. Finally, the validity of this method is verified by computer simulation and real experiment.

INDEX TERMS Line scan camera (LSC), calibration, space rings group (SRG), local-Canny-PAE (LCPAE), two-step particle swarm optimization (TS_PSO).

I. INTRODUCTION

LINE scan camera (LSC) is widely used in industrial production for real-time detection of moving objects, because of its advantages of high resolution and continuous high-speed measurement. In these applications, especially in three-dimensional (3D) surface reconstruction and the measurement of the accuracy of moving objects, the internal parameters of the visual system often need to be pre-acquired. So, the calibration of camera is an indispensable process.

The existing calibration methods are mostly designed for the matrix camera [1], [2], for the LSC is very limited. Therefore, it is significant to design a simple and effective calibration method for LSC.

Because of its unique one dimensional imaging characteristics, LSC is difficult to obtain the complete geometric information such as corners and contours, making it difficult to calibrate. Therefore, the calibration of the LSC usually need to solve the following problems:

- Calibration target design effectiveness. Due to the one-dimensional scanning imaging characteristics of LSC, it is difficult to obtain effective external geometric information at one time. Therefore, the design of the calibration target must allow the camera to detect the target content and clearly distinguish the information of calibration features.
- The rationality of solving the model. The ideal LSC conforms to the Pinhole model. However, the real camera lenses often contain distortions, and the distortion effects cannot be ignored when the visual system needs higher accuracy. In addition, the effectiveness of the image point information extraction algorithm has great influence on the calibration result.
- Calibration method of operability. In practice, since the camera and other equipment often need to be adjusted according to the scene, the calibration method of the camera is required to have higher portability and operability.

Currently, the calibration methods for LSC can be roughly classified into two types: the dynamic scanning calibration method and the static calibration method.

Dynamic calibration method mostly through the relative motion between the camera and the calibration target, to get the complete target pattern information. This method usually needs to set or acquire the relative motion information in advance, and accurate and reliable motion control is required in the calibration process. Drareni *et al.* [4] obtains the scanning image of camera by using a planar grid pattern and Hui [5]–[7] presents a series of scanning calibration methods using 3D patterns instead of planar patterns, etc.

According to the one-dimensional imaging characteristics of LSC, the static calibration methods usually establish a correspondence between the target and the image by constructing a pattern such as parallel lines or blocks. Horaud *et al.* [3] firstly proposed this kind of calibration method. However, the pattern must be translated in the direction of the coordinate axis with known steps, the result of the calibration depends on the accuracy of the panning control.

The static calibration method has high operability and portability, and simple to calculate compared with the dynamic scanning method. Moreover, since the dynamic calibration method needs additional control costs, the calibration result is easily affected by the movement accuracy. However, the static calibration involves solving multi-parameter equations, and needs to obtain a plurality of non-collinear spatial point information.

Sun [8]–[10] acquired non-collinear feature points by shooting target patterns from multiple angles using a combination of matrix camera and LSC. Luna *et al.* [11] and Lilienblum *et al.* [12], [13] build the spatial target model through 3D target forms. The 3D target method is more computationally simple and avoids the introduction of matrix camera errors. However, the actual straight line is usually a narrow band whose width information is not ideal. The ideal straight line feature appears as a single point on the LSC image, which increases the positioning difficulty of the image feature. Li *et al.* [14] changes the line to a triangle block with bandwidth information instead of a line style, the effective utilization area of the target pattern and the final result of calibration is easily affected by the tilt angle of the triangle.

In view of the above factors, a static calibration method based on 3D right-angle stereo target with concentric rings is presented for surface measurement, namely space rings group (SRG). The method uses concentric ring symmetrical structure graph to reduce the calculation difficulty in the calibration process and increase the number of effective points in the interval.

Usually, the real camera imaging model is nonlinear. In order to avoid the instability of optimization results caused by the correlation of parameter calculations and to speed up the optimization, a two-step method is used to solve and optimize the calculation of parameters. In addition, since the effectiveness of the image point location algorithm has a direct impact on the calibration results, a sub-pixel location algorithm is proposed in this paper. Through the use of global Canny operator and local partial area effect (Local-Canny-PAE, LCPAE) algorithm for regional step-by-step positioning, the image feature location speed and accuracy are improved.

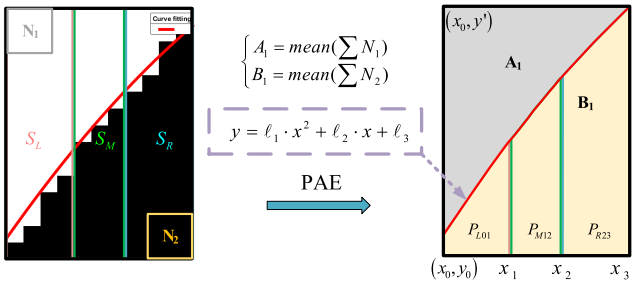

FIGURE 1. Equivalent integral of PAE.

The paper consists of the following parts: Part II, using BM3D [22] filtering to remove noise and obtaining the sub-pixel edge position with LCPAE. Part III, using the Space Rings Group (SRG) target model to statically calibrate a LSC. Part IV, optimizing the calibration parameters using the Two-step particle swarm optimization (TS_PSO) algorithm. Part V and Part VI, validation and analysis of calibration results, including computer simulation experiments and real calibration experiments. Part VII, Calibration Model Summary.

II. A SUB-PIXEL EDGE DETECTION ALGORITHM

For the static calibration of the line camera, it is necessary to acquire the feature end positions of line segments. In order to reduce the effects of noise and system signal transmission instability, multiple lines of statically scanned images are often used for calibration. Thanks to the characteristic that the feature endpoints present line shapes on multi-line scan images, the position information of the endpoints can be easily obtained by means of sub-pixel detection.

There are many existing sub-pixel edge detection methods such as interpolation, moment method [15], [16], fitting method [17] and other methods [18]–[20]. The interpolation method is simple and computationally fast, but the accuracy of the acquired edges is low. Compared with the interpolation method, moment estimation method [15], [16] can obtain higher positioning accuracy, but the algorithm is still easy to be disturbed by noise. In addition, these methods can't accurately obtain the edge point intensity value and direction of change. Moreover, the computational complexity is high for the above methods.

Fortunately, Trujillo-Pino *et al.* [21] proposed an edge location method based on partial area effect (PAE), which can precisely detect the edge at a sub-pixel position. The method is accuracy in the description of the edge features.

The edge is simulated by PAE, which using equivalent integral to calculate the strength of the two sides of the second-order curve in a neighborhood, and as shown in Fig. 1.

$$S_L = ((x_1 - x_0) \cdot (y' - y_0) - P_{L01}) \cdot A_1 + P_{L01} \cdot B_1 \quad (1)$$

The intensities of the three sub-window areas are S_L, S_M, and S_R, respectively. A_1 and B_1 are the mean values of the

intensities of the diagonal regions N_1 and N_2 within the window.

$$P_{L01} = \int_{x_0}^{x_1} (\eta_1 \cdot x^2 + \eta_2 \cdot x + \eta_3) dx \tag{2}$$

Where P_{L1}, P_{M01}, and P_{R01} are respectively the area of the area below the quadratic curve in the three sub-windows. η_1, η_2, and η_3 are the coefficients of the curve to be fitted.

However, the PAE algorithm calculates the entire image at the sub-pixel level, and the calculation based on the region easily covers the noise information. In other words, the method of PAE has to face the follow tough questions:

- The PAE method acts on the entire image to detect the sub-pixel edges, in particular, which involves the calculation of complex windows, which undoubtedly increased the cost of computing.
- The calculation results are easily affected by the noise in the window area, especially, salt and pepper noise and white Gaussian noise.
- The appropriate threshold selection is also the key to positioning accuracy, especially when the local edge information in the image is not obvious.

An improved PAE-based method, LCPAE is proposed to solve the above problem, and the flow is shown in Fig.2. In order to reduce the time consumption of PAE, the LCPAE method firstly uses Canny for pixel-level edge detection and then uses PAE for sub-pixel level detection in a small local window. The LCPAE method uses Canny for pixel-level edge detection in the global region and then uses PAE for sub-pixel level detection in a local regions.

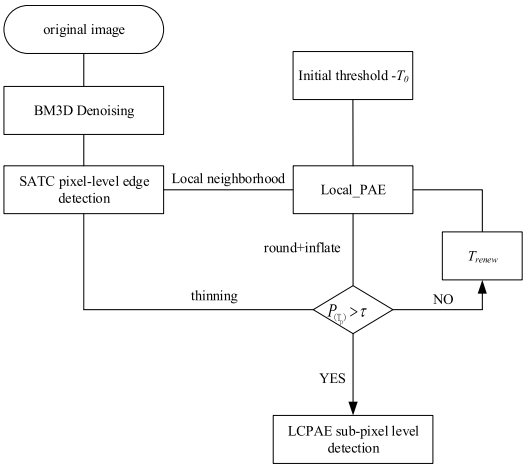

FIGURE 2. The flow chart of sub-pixel edge detection.

Firstly, BM3D [22] algorithm is used to remove the image noise, and the self-adaptive threshold Canny (SATC) edge detection that proposed by Tang *et al.* [23] is used for the edge detection at pixel level, and the automatic threshold selection method based on gradient amplitude histogram and maximum variance between classes. SATC can extract real edges better for different images, especially for low contrast images. With the SATC algorithm, it can capture pixel-level edges and help set thresholds for the improved PAE algorithms of LCPAE.

Secondly, it takes the edge point of SATC as the core of a neighborhood window and LCPAE is operated inside the window. The optimal threshold is determined by calculating the correlation between the results of PAE at different thresholds and the SATC, as shown in Fig.3.

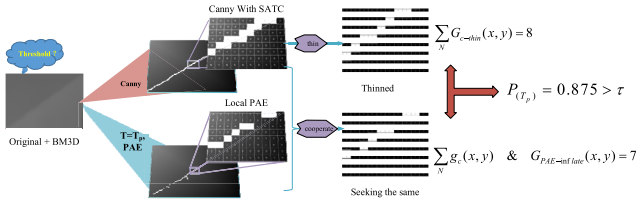

FIGURE 3. The threshold calculation of LCPAE.

SATC uses Eq. (3) to get the pixel-level edges:

$$g_c(x, y) = Canny(f(x, y), Adp\_T_{1,2}) \tag{3}$$

Where $f(x, y)$ represents the input image, $Adp\_T_{1,2}$ are the thresholds of SATC, g_c $(\cdot)$ denotes a binary image that generated by SATC.

What LCPAE needs to get is the specific location information of the edge. However, the edge provided by the SATC is relatively rough. So, the edge of SATC needs to be refined by Eq. (4):

$$G_{c-thin}(x, y) = (g_c \otimes b)(x, y) \tag{4}$$

Where G_{c-thin} $(\cdot)$ stands for the image of g_c $(\cdot)$ after convolution thinning operation by structural unit b. Otherwise, $\otimes$ represents morphological refinement.

The PAE model obtains the sub-pixel edge. In order to facilitate the assessment of the threshold T_p applicability, the edge information needs to be rounded by Eq. (3):

$$I_{Local}(x, y) = round(LPAE_{(T_p)}(f(x, y))) \tag{5}$$

The Local-PAE method is $LPAE_{(TP)}(\cdot)$ that based on T_P, and T_P expresses a corresponding threshold. $LPAE_{(TP)}(\cdot)$ will return a sub-pixels collinear. *round* $(\cdot)$ will return a rounded integer of sub-pixel collinear. $\mathrm{I}_{Local}(\cdot)$ states the local neighborhood result of output that a binary image generated by PAE edge detection.

The rounding result of $\mathrm{I}_{Local}(\cdot)$ will reduce the coverage of the edge information. In order to reduce the error, the $\mathrm{I}_{Local}(\cdot)$ is expanded by Eq. (6).

$$G_{PAE-\mathrm{inf}\,late}(x, y) = (I_{Local(T_p)} \oplus b')(x, y) \tag{6}$$

Where $G_{PAE-inflate}(\cdot)$ represents the local PAE edge after rounding and expansion. Besides, $\otimes$ represents morphological expansion.

The applicability of the threshold T_p is judged by Eq. (7). The new threshold is updated with Eq. (8) and Eq. (9):

$$P_{(T_p)} = \frac{\sum\limits_N g_c(x, y) \;\&\; G_{PAE-\mathrm{inf}\,late}(x, y)}{\sum\limits_N G_{c-thin}(x, y)} \tag{7}$$

$P_{(TP)}$ indicates the correlation of SATC and Local-PAE at a threshold of T_P.

$$S_{feedback} = \begin{cases} 1 & P_{(T_p)} > \tau \\ 0 & other \end{cases} \tag{8}$$

And

$$T_{renew} = T_p - l \cdot S_{feedback} \tag{9}$$

The judgment threshold is τ to verify the validity of T_P, and T_{renew} is the updated threshold in Local-PAE. l indicates the update iteration step.

III. SPACE RINGS GROUP (SRG) CALIBRATION METHOD

A. LINE SCAN CAMERA MODEL

In the process of calibration of a line scan camera, the camera is calibrated by a combination of a linear model and a non-linear model, as shown in Fig.4. First of all, by using the linear model to obtain the initial parameter solution, and then use the non-linear model to optimize the iteration, to obtain the final optimization of all the parameters of the solution.

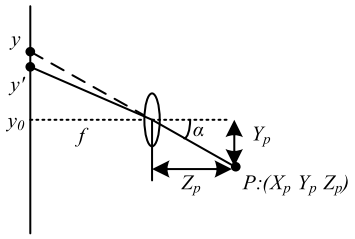

FIGURE 4. The model of Line scan camera.

The space point is P, and the coordinates of the camera coordinate system (CCS) is (X_P, Y_P, Z_P).y denotes the undistorted mapping point on the image under the linear model, and y' represents the distortion map point on the image under nonlinear model. y_0 stands for the main point. f means the focal length. The linear model can be expressed as follows:

$$\begin{cases} y = y_0 + f \cdot g(\alpha) \\ g(\alpha) = \tan(\alpha) = \frac{Y_P}{Z_P} \end{cases} \tag{10}$$

The distortion parameters k_1, k_2, k_3 [24] are considered in the nonlinear model. It is still used f to indicate the camera focal length. And the line scan camera imaging model can be expressed as follows:

$$\begin{cases} y' - y_0 + k_1 \cdot (y - y_0)^2 + k_2 \\ \cdot (y - y_0)^3 + k_3 \cdot (y - y_0)^5 = f \cdot \tan(\alpha) \\ X_P = 0 \end{cases} \tag{11}$$

The relationship between the world coordinate system (X_P^W, Y_P^W, Z_P^W) and the camera coordinate system (X_P, Y_P, Z_P) can be expressed as follows:

$$\begin{bmatrix} X_P \\ Y_P \\ Z_P \end{bmatrix} = \begin{bmatrix} R & T \end{bmatrix} \cdot \begin{bmatrix} X_P^w \\ Y_P^w \\ Z_P^w \\ 1 \end{bmatrix} = \begin{bmatrix} R_1 & T_1 \\ R_2 & T_2 \\ R_3 & T_3 \end{bmatrix} \cdot \begin{bmatrix} X_P^w \\ Y_P^w \\ Z_P^w \\ 1 \end{bmatrix} \tag{12}$$

Where R is the rotation matrix, and T means the translation matrix; R_1, R_2, R_3, T_1, T_2 and T_3 are their component.

Otherwise, the linear model of a line scan camera in the world coordinate system is:

$$\begin{cases} 0 = r_{11} \cdot X^W + r_{12} \cdot Y^W + r_{13} \cdot Z^W + T_1 \\ y = y_0 + f \cdot S_y \end{cases} \tag{13}$$

Similarly, the nonlinear model can also be represented as follows:

$$\begin{cases} 0 = r_{11} \cdot X^W + r_{12} \cdot Y^W + r_{13} \cdot Z^W + T_1 \\ y' = y_0 + f \cdot (S_y + a_1 \cdot S_y^2 + a_2 \cdot S_y^3 + a_3 \cdot S_y^5) \end{cases} \tag{14}$$

Where

$$S_y = \frac{r_{21} \cdot X^W + r_{22} \cdot Y^W + r_{23} \cdot Z^W + T_2}{r_{31} \cdot X^W + r_{32} \cdot Y^W + r_{33} \cdot Z^W + T_3} \tag{15}$$

B. SPACE RINGS GROUP (SRG) PATTERN

The SRG target pattern, mainly consists of two parts: rings group and regional labels. The rings group is used to generate the space points, and the labels eliminate the ambiguity of the calculation plane by determining the quadrant area of the target pattern in time-space calibration, and it as shown in Fig.5.

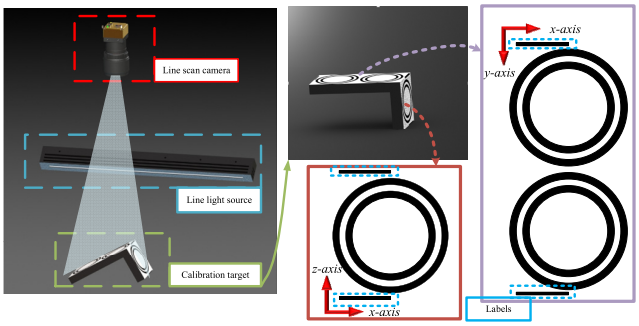

FIGURE 5. The 3D view of Calibration target.

The Line_1 and Line_2 are the intersection of scanning plane and space target of line camera in different positions in Fig.6. And it can be seen from the Fig.6 that Line_1 contains the labels, Line_2 does not contain. When Line_1 removes the label information, the result of the static scan of the multi-line intersections in the two positions is the same, which adds the ambiguity information to the calculation of the subsequent scan plane equation. By using the regional labels, not only the calibration range is increased, but also ambiguous information is eliminated.

C. THE CALCULATION OF SCANNING PLANE OF THE CAMERA

The line scan camera's plane can be solved by L_{xy} and L_{xz}. Meanwhile, the rotation vector R_1 and the translation parameter T_1 can also be obtained from the plane equation. The linear equations of L_{xy} and L_{xz} can be solved by calculating the distance (h_1, h_2, h_3) between the straight line to the circle

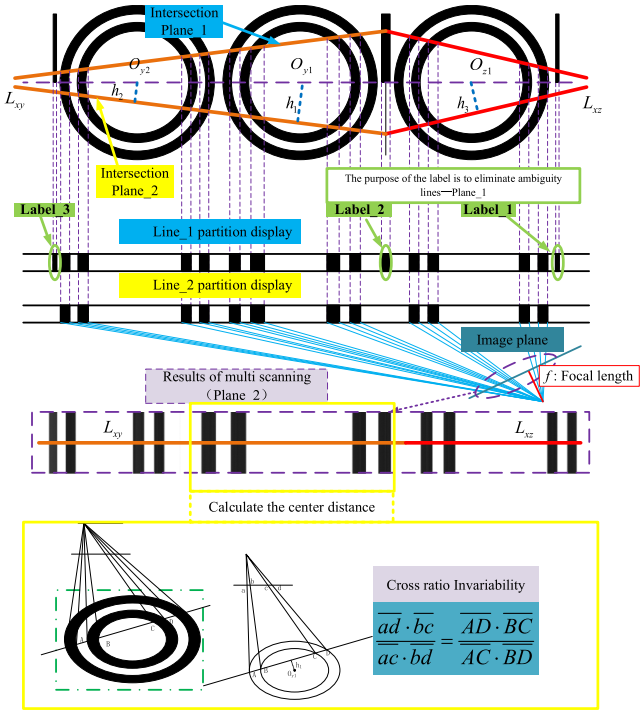

FIGURE 6. The Line-scan camera images of the target.

center of the torus calculated by the invariance property of the space beam. Combined with regional labels, to further determine the final results. The invariance properties of the space beam [25] are also be shown in Fig.6.

The mapping points of the target feature points (*A, B, C, D*) in the image are (*a, b, c, d*), the image of line scan can be approximate to a line, so a function can be expressed:

$$\frac{\overline{ad}\cdot\overline{bc}}{\overline{ac}\cdot\overline{bd}}=\frac{(y_a-y_d)\cdot(y_b-y_c)}{(y_a-y_c)\cdot(y_b-y_d)} \tag{16}$$

Where (y_a, y_b, y_c, y_d) are the corresponding image pixel coordinates of (*A, B, C, D*) under the linear model. The distance from the center of the circle to (*A, B, C, D*) is (r_a, r_b, r_c, r_d). And h is the distance from the line to the center of the circle:

$$\begin{aligned}&\frac{(y_a-y_d)\cdot(y_b-y_c)}{(y_a-y_c)\cdot(y_b-y_d)}\\&=\frac{\left(\sqrt{r_a^2-h^2}+\sqrt{r_d^2-h^2}\right)\cdot\left(\sqrt{r_b^2-h^2}+\sqrt{r_c^2-h^2}\right)}{\left(\sqrt{r_a^2-h^2}+\sqrt{r_c^2-h^2}\right)\cdot\left(\sqrt{r_b^2-h^2}+\sqrt{r_d^2-h^2}\right)}\end{aligned} \tag{17}$$

Linear equations of L_{xy} can be set as:

$$L_{xy}:\begin{cases}\mu_1\cdot X+\mu_2\cdot Y+1=0\\ Z=0\end{cases} \tag{18}$$

The coordinates of two circle centers corresponding to the rings groups are $(0, O_{y1}, 0)$ and $(0, O_{y2}, 0)$, and

$$\begin{cases}\dfrac{|\mu_2\cdot O_{y_1}+1|}{\sqrt{\mu_1^2+\mu_2^2}}=h_1\\ \dfrac{|\mu_2\cdot O_{y_2}+1|}{\sqrt{\mu_1^2+\mu_2^2}}=h_2\end{cases} \tag{19}$$

Where h_1 and h_2 are the distances from the straight line to the two center points, and the symbols of μ_1 and μ_2 can be determined by the labels.

The linear equation of L_{xz} can be solved by the intercept $L_d = 1/\mu_1$ of the linear equation L_{xy} on the X axis and the distance to the center of the rings group $(0, 0, O_{z1})$, the equation of L_{xz} can be obtained from L_d and h_3, expressed as follow:

$$L_{xz}:\begin{cases}\mu_1\cdot X+\mu_3\cdot Z+1=0\\ Y=0\end{cases} \tag{20}$$

And

$$\frac{|\mu_3\cdot O_{z_1}+1|}{\sqrt{\mu_1^2+\mu_3^2}}=h_3 \tag{21}$$

In summary, the camera scanning plane is:

$$\mu_1\cdot X+\mu_2\cdot Y+\mu_3\cdot Z+1=0 \tag{22}$$

D. THE CALCULATION OF INTERNAL PARAMETERS

When the line camera plane intersects all circles, the information of twenty-four feature points can be acquired for the camera parameter calibration.

Firstly, the initial solution of the calibration parameters is obtained from the non-distorted linear model of the line camera:

$$\begin{cases}0=R_{11}\cdot X^W+R_{12}\cdot Y^W+R_{13}\cdot Z^W+T_1\\ y=y_0+f_y\cdot\frac{R_{21}\cdot X^W+R_{22}\cdot Y^W+R_{23}\cdot Z^W+T_2}{R_{31}\cdot X^W+R_{32}\cdot Y^W+R_{33}\cdot Z^W+T_3}\end{cases} \tag{23}$$

The equation can be simplified as:

$$y=\frac{L_1\cdot X^W+L_2\cdot Y^W+L_3\cdot Z^W}{L_4\cdot X^W+L_5\cdot Y^W+L_6\cdot Z^W} \tag{24}$$

Introducing four intermediate variables (ω, s_1, s_2, s_3), where s_1, s_2, and s_3 represent the proportion coefficient between the parameters:

$$\begin{cases}y_0=s_1*T_1\\ T_2=s_2*T_1\\ T_3=s_3*T_1\end{cases} \tag{25}$$

And ω is the scaling factor of the simplified equation, the relationship between the parameters can be expressed by the

following equations:

$$\begin{cases} L_1 = \omega \cdot (f_y \cdot r_{21} + s_1 \cdot r_{31} - s_2 \cdot r_{11}) \\ L_2 = \omega \cdot (f_y \cdot r_{22} + s_1 \cdot r_{32} - s_2 \cdot r_{12}) \\ L_3 = \omega \cdot (f_y \cdot r_{23} + s_1 \cdot r_{33} - s_2 \cdot r_{13}) \\ L_4 = \omega \cdot (r_{31} - s_3 \cdot r_{11}) \\ L_5 = \omega \cdot (r_{32} - s_3 \cdot r_{12}) \\ L_6 = \omega \cdot (r_{33} - s_3 \cdot r_{13}) \end{cases} \tag{26}$$

Establish a linear system of equations between the space point coordinates and the image coordinates, and then obtain the values of $L_i (i = 1, \cdots 6)$ by means of singular value decomposition (SVD), and calculate the values of parameters as (27), as shown at the bottom of this page, where R_1 and T_1 can be solved by the plane equation (22):

$$\begin{bmatrix} r_{11} \\ r_{12} \\ r_{13} \\ T_1 \end{bmatrix} = \frac{\pm 1}{\sqrt{\mu_1^2 + \mu_2^2 + \mu_3^2}} \begin{bmatrix} \mu_1 \\ \mu_2 \\ \mu_3 \\ 1 \end{bmatrix} \tag{28}$$

The sign of T_1 can be determined by whether the image contains the regional labels, it should be $T_1 < 0$ when the area of the rings group does not contain the labels.

Otherwise, the relationship between ω and R_3 is as follows:

$$\omega = R_3 \cdot \begin{bmatrix} L_4 \\ L_5 \\ L_6 \end{bmatrix} \tag{29}$$

For convenience, the intermediate variable ε is introduced as follows:

$$\varepsilon = R_1 \cdot \begin{bmatrix} L_4 \\ L_5 \\ L_6 \end{bmatrix} = -\omega \cdot s_3 \tag{30}$$

and

$$L_4 = \omega \cdot r_{31} - \varepsilon \cdot r_{11} \tag{31}$$

Where ω has:

$$\begin{aligned} \omega^2 &= \omega^2 \cdot (r_{31}^2 + r_{32}^2 + r_{33}^2) \\ &\Rightarrow \omega^2 = (L_4 + \varepsilon \cdot r_{11})^2 + (L_5 + \varepsilon \cdot r_{12})^2 + (L_6 + \varepsilon \cdot r_{13})^2 \end{aligned} \tag{32}$$

And the rotation vector R_2 is:

$$R_2 = R_1 \times R_3 \tag{33}$$

All of the initial values of parameters can be found at this step, but they are not the final accurate results. The linear model does not take into account the distortion, and the plane (μ_1, μ_2, μ_3) is also not a convincing plane of scanning.

IV. OPTIMIZATION

A. TWO-STEP PARTICLE SWARM OPTIMIZATION (TS_PSO)

In the process of calibration of a line scan camera, the camera is calibrated by a combination of a linear model and a non-linear model, as shown in Fig.4. First of all, by using the linear model to obtain the initial parameter solution, and then use the non-linear model to optimize the iteration, to obtain the final optimization of all the parameters of the solution.

In the linear model, all the calibration parameters are initially determined. However, this is not the final result. Due to the fact that the camera lens often contains distortion, the imaging model is nonlinear, which affecting the accuracy of the edge detection of the feature points, resulting in calibration results error.

In order to get as accurate calibration parameters as possible, it needs to optimize the model. However, there are many problems to be faced in the optimization of multi parameters. One hand, the amount of calculation is large, the stability of the optimization results is poor. The real camera imaging model is nonlinear, and calculations between internal parameters are interrelated. If all parameters are optimized directly, which easily leads to non-convergence of optimization. Otherwise, the initial optimization range of the parameters cannot be determined because of the different magnitudes of the actual parameters. On the other hand, the optimization process tends to fall into the local optimal solution. Because of the influence of each parameter on the calibration result is not the same. Such as the distortion of the lens is very small, which has limited influence on the calibration result. Indiscriminate optimization of all parameters at the same time, will ignore the impact of certain parameters, resulting in its optimization results into a local optimum. For the purpose of overcome these problems, it is necessary to perform differentiating optimization for different parameters, and two-step particle swarm optimization (TS_PSO) is a good choice.

TS_PSO consists of two parts: In the first step, the distortion of the lens has limited influence on the calibration result, so distortion parameters can be ignored, and the nonlinear model used for camera solving is converted to linear model. The initial solution of the parameter is obtained by linear model, and the optimal range is given. Then, the initial optimization solution is obtained by optimizing (h_1, h_2, h_3) in the initial parameters. In the second step, by introducing the distortion parameters, a nonlinear model is established to limit the optimization range. And then the particle swarm optimization (PSO) algorithm is optimized for the initial optimization solution to obtain the final optimization solution,

$$\begin{bmatrix} X_1^W & Y_1^W & Z_1^W & -y_0 \cdot X_1^W & -y_0 \cdot Y_1^W & -y_0 \cdot Z_1^W \\ X_2^W & Y_2^W & Z_2^W & -y_0 \cdot X_2^W & -y_0 \cdot Y_2^W & -y_0 \cdot Z_2^W \\ \vdots & \vdots & \vdots & \vdots & \vdots & \vdots \\ X_n^W & Y_n^W & Z_n^W & -y_0 \cdot X_n^W & -y_0 \cdot Y_n^W & -y_0 \cdot Z_n^W \end{bmatrix} \begin{bmatrix} L_1 \\ L_2 \\ L_3 \\ L_4 \\ L_5 \\ L_6 \end{bmatrix} = 0 \tag{27}$$

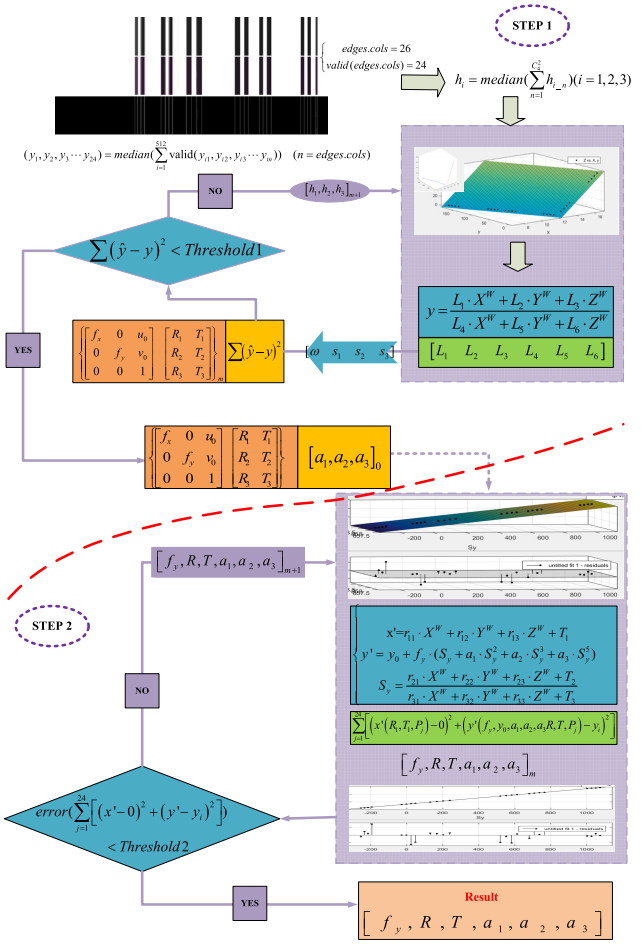

FIGURE 7. The Two-step particle swarm optimization (TS_PSO).

as shown in Fig.7.

In Fig.7, the first step optimization is aiming at the scanning plane (μ_1, μ_2, μ_3), because the error is mainly caused by (h_1, h_2, h_3), and which will be calculated by the sub-pixel location.

However, the distortion, the blurred depth of field and the position of the sub-pixel feature points on the image can't accurately reflect the cross-ratio property, thus affecting the accuracy of the scanning plane. The second step is an optimization for all parameters $[f_y, R, T, a_1, a_2, a_3]$, and the initial values $[a_1, a_2, a_3]$ of the distortion coefficients can be obtained from the first step.

The PSO [26] is a global optimization algorithm that produces random particles in an optimized space and calculates the fitness function at different particle locations. Each particle according to its own and global applicability, to change their position for the next iteration update. When all the particles converge, the optimal solution is finally found. The particle updates its speed and position through the equation expressed as:

$$\begin{cases} V_{in}^{k+1} = \eta \cdot V_{in}^{k} + c_1 \cdot \lambda_1 \cdot (\Phi_{in}^{k} - \xi_{in}^{k}) + c_2 \cdot \lambda_2 \cdot (\Gamma_{in}^{k} - \xi_{in}^{k}) \\ \xi_{in}^{k+1} = \xi_{in}^{k} + V_{in}^{k+1} \end{cases} \tag{34}$$

TABLE 1. Computer simulation parameters of calibrated targets.

r_1 (mm)	r_2 (mm)	r_3 (mm)	r_4 (mm)	O_{y1} (mm)	O_{y2} (mm)	O_{z1} (mm)	ANGLE
45	40	35	30	(0,50,0)	(0,145,0)	(0,0,50)	90°

TABLE 2. Computer simulation parameters of the camera.

f_y (pixel)	y_0 (pixel)	φ_1	φ_2	φ_3	T_1 (mm)	T_2 (mm)	T_3 (mm)
3500	1200	$3\pi/10$	$-\pi/36$	0	-12.8211	-10	300

Where $\xi_i = (\tau_{i1}, \tau_{i2}, \cdots, \tau_{iN})$ represents a N dimension vector of current particle position in the search space. $(\tau_{i1}, \tau_{i2}, \cdots, \tau_{iN})$ stands for the optimized parameters and $i$is the serial number of particle. $V_i = (v_{i1}, v_{i2}, \cdots v_{iN})$ is the velocity of particle swarm, and the local extreme is $\Phi_i = (\phi_{i1}, \phi_{i2}, \cdots, \phi_{iN})$, the global extreme is $\Gamma_i = (\zeta_{i1}, \zeta_{i2}, \cdots, \zeta_{iN})$. Otherwise, η signifies the weight, k means the iteration times, c_1 and c_2 are acceleration coefficients, λ_1 and λ_2 are the random numbers at the range of 0-1.

B. THE PROCEDURE OF CALIBRATION

The entire calibration procedure is shown in Fig.8.

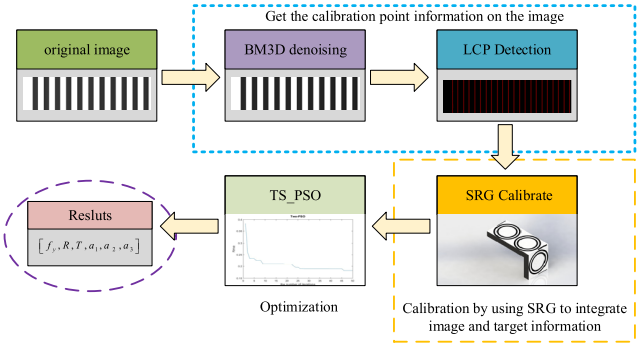

FIGURE 8. The process steps of Calibration.

V. THE COMPUTER SIMULATIONS

The proposed calibration method has been tested by computer simulated data and real data. The computer simulated data are used to evaluate the calibration performances considering the following four factors: (1) the sub-pixel location accuracy; (2) the depth of field and the noise level for locating the image points; (3) the lens distortion; (4) the placement of calibration target. The real data are used for verifying the practicability of the method.

The calibration target information includes four radius of every rings group $[r_1, r_2, r_3, r_4]$, the circle center coordinate (O_{y1}, O_{y2}, O_{z1}), and the space angle between two target planes. The computer simulated target parameters are shown in the following Table. 1.

The camera parameters is simulated and shown in Table. 2. Firstly, the linear imaging model is derived from

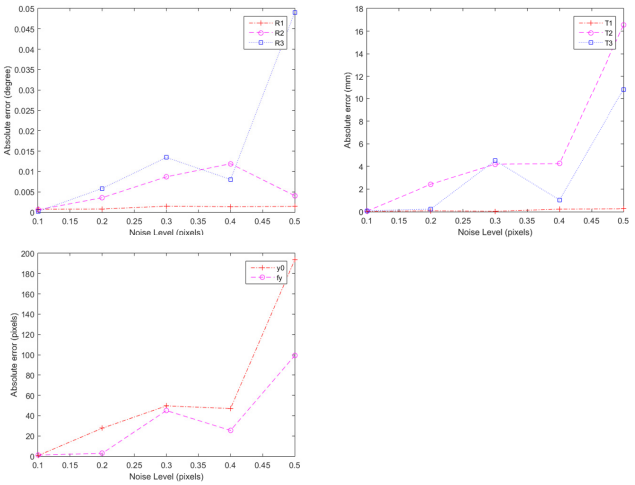

FIGURE 9. Calibration results under real projection point data with noises.

parameters (f_y, R, T), and the coordinates of twenty-four intersection points are obtained, and R is the rotation matrix generated by the rotation angle $(\varphi_1, \varphi_2, \varphi_3)$. Secondly, noises are added to the derived simulated image sub-pixel points. Thirdly, the theoretical simulated image points is sub-pixels but the edge points of image are not. In order to simulate the true pixel points of image, the CCD photosensitive unit is simulated by rectangle area integral, and the real image is generated. Otherwise, white Gaussian noises and Gaussian blur are added to the simulated image, considering that the signal noise and depth of field. Fourthly, the mapping range of the target in different space distance is different, resulting in a different influence on the accuracy of edge detection. The different spatial positions of the target are simulated by changing T_3. Fifthly, the lens distortion is an extra factor which is taken into account. Finally, the all simulated images and the derived simulated image points are used to work out the intrinsic and extrinsic camera parameters by the method in Section IV.

A. PERFORMANCE WITH RESPECT TO THE NOISE LEVEL FOR INTERSECTION POINTS

The true intersection points are projected onto the image plane by (f_y, R, T). In order to test the influence of sub-pixel positioning accuracy on calibration results, Gaussian noise with 0 mean and σ standard deviation is added to the true projected points. And the estimated camera parameters are then compared with the true values in Table 2. The absolute error is measured for the estimated camera parameters. The noise level is varied by changing σ from 0.1 to 0.5 pixels in 0.05 pixels increment. For each noise level, 100 independent trials are performed and the average results are shown in Fig.9.

It can be seen from Fig.9 that $(R_2, R_3, T_2, T_3, f_y, y_0)$ are sensitive to the noise level for intersection points. And with the increase of noise, the calculation errors also tend to increase.

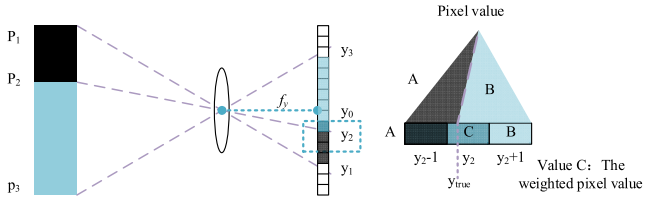

FIGURE 10. The simulation of image pixel values.

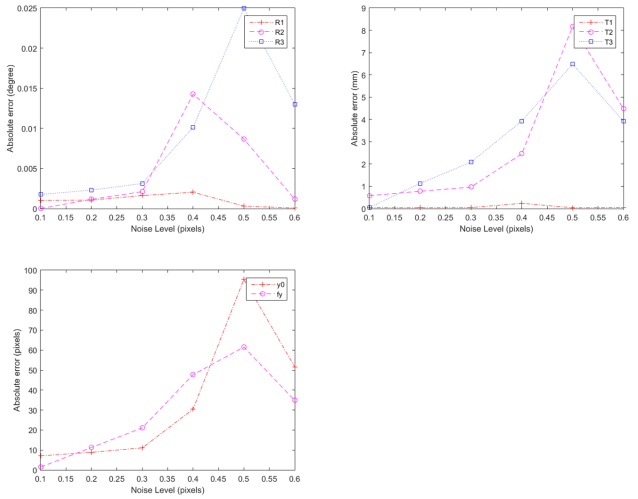

FIGURE 11. Calibration results under simulated images with noises.

B. PERFORMANCE WITH RESPECT TO THE NOISE LEVEL FOR IMAGE

The theoretical simulated image points can be accurate to decimal but the description of image points are not, as shown in Fig.10. In order to simulate the CCD photosensitive unit, a rectangle area integral is used, the results are used for further experiments.

Otherwise, considering that the signal noise and depth of field, white Gaussian noises and Gaussian smoothing fuzzy are added to the simulated image, and the noise level is varied by changing σ from 0.1 to 0.6 pixels in 0.1 increment and the coefficient of Gaussian- smooth is 0.5. For each noise level, 100 independent trials are performed and the average results are shown in Fig.11.

Where $(R_2, R_3, T_2, T_3, f_y, y_0)$ are also sensitive to the noise level for image in Fig.11. And with the increase of noise, the calculation errors also tend to increase. It also can be seen that the influence of image noise on the calibration accuracy has a positive correlation with the sub-pixel detection from Fig.11.

C. PERFORMANCE WITH RESPECT TO THE DIFFERENT SPATIAL

The different spatial positions of the target are simulated by changing T_3. The relative position of the target relative to the camera has a certain randomness to the calibration results from Fig.12. Taking into account the target size and the

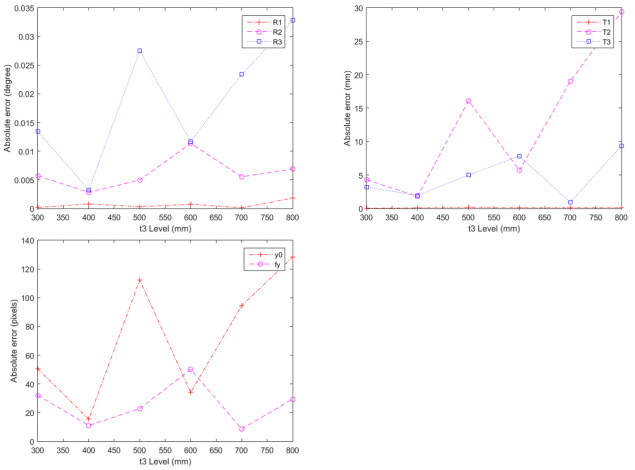

FIGURE 12. Calibration results at different T_3 positions.

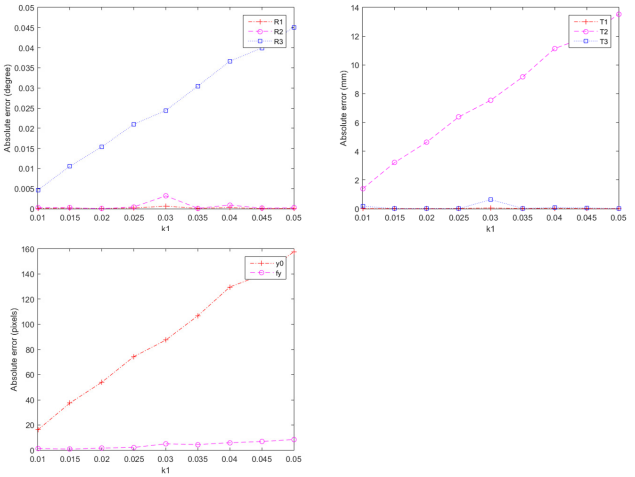

FIGURE 13. The Line-scan camera images of the target.

number of pixels the camera imaging, and calibration error and the relationship between the sub-pixel detection accuracy. It is considered that the resolution of the target in the imaging plane is different under different spatial positions, and the detection accuracy of sub-pixels is different, thereby affecting the calibration accuracy.

D. PERFORMANCE WITH RESPECT TO THE DIFFERENT DISTORTION PARAMETERS

By setting the parameters k_1 to introduce camera distortion, and using non-linear model for simulation. The simulated camera model is determined by Eq. (1).

In Fig.13, the lens distortion have an impact on (y_0, T_2, T_3), with the distortion coefficient increases, the absolute error also becomes larger. The optimization process has significant effects on $(R_1, R_2, T_1, T_3, f_y)$.

VI. REAL EXPERIMENT

SRG method is used to conduct real calibration experiments in different locations. The experimental results are divided

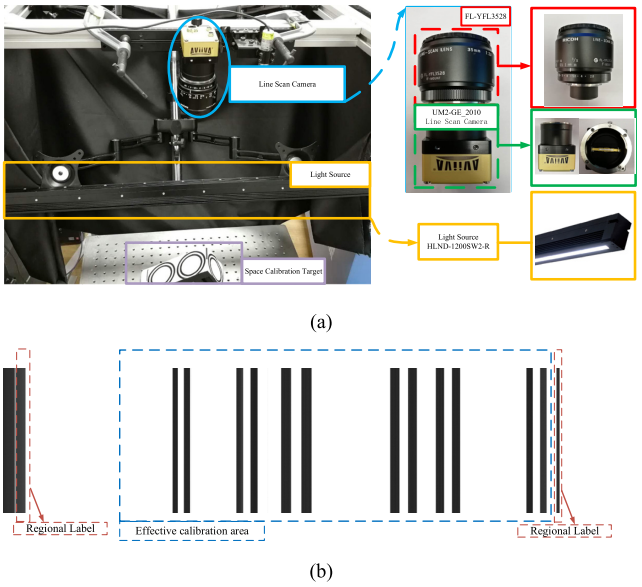

FIGURE 14. (a) The layout of Calibration experiment (b) The image of 500 lines under static scanning.

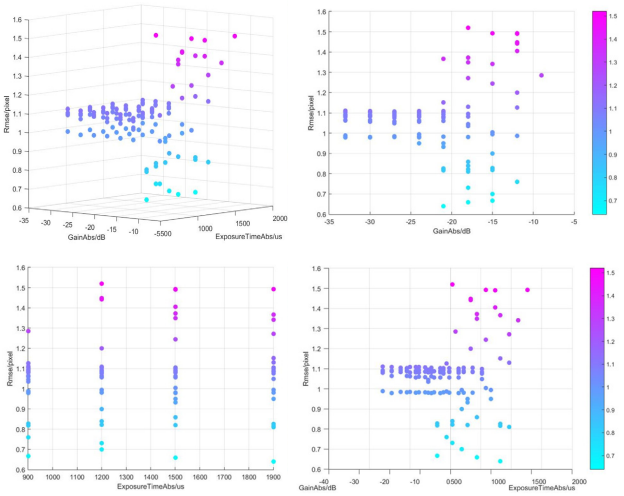

FIGURE 15. The non-optimized results.

into six groups according to different angles. The equipment models as shown in Fig.14 (a). Each image is the result of five hundred static scans, as shown in Fig.14 (b). The experimental camera is UM2-GE_2010, the lens is FY-YFL3528, and the light source is HLND-1200SW2-R. In order to consider the impact of background factors, each experiment was performed at different exposures and gains to obtain valid experimental data, the non-optimized results are shown in Fig.15.

In Fig.15, the non-optimized results for each group at different exposures and gains clearly show that improper exposure and gain can severely affect the calibration results. When choosing a reasonable exposure and gain range, the initial non-optimized RMSE (root mean square error) can be controlled within 0.9.

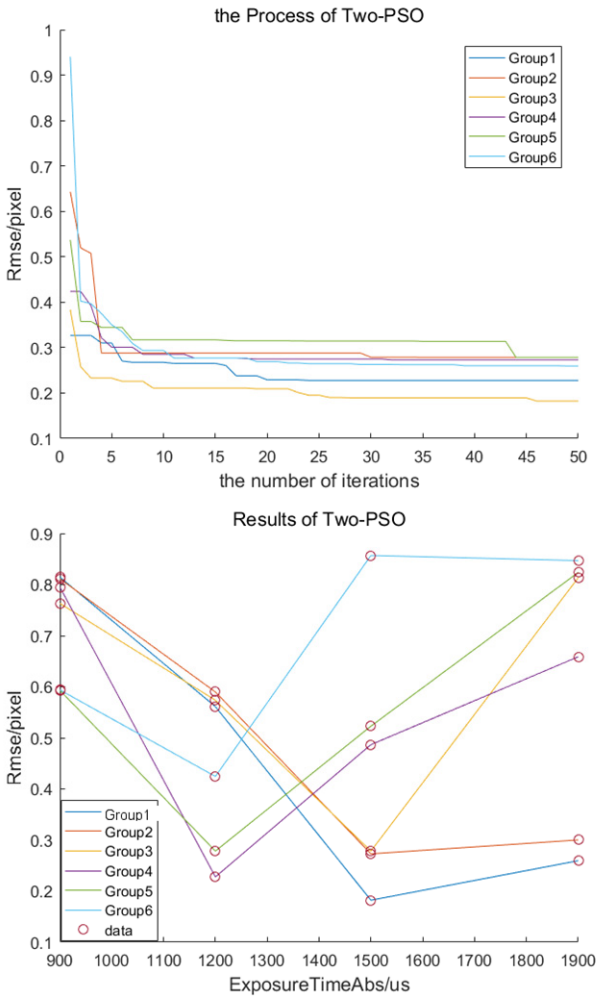

FIGURE 16. The optimized results after TS_PSO.

Taking into account other factors such as lens distortion, the TS_PSO method is used to optimize the results in the reasonable exposure and gain interval of Fig.15. The three axes are exposure time (us), gain (dB), and RMSE (pixel). Otherwise, the optimization process and results are shown in Fig.16.

In Fig.16, after TS_PSO optimization, RMSE can be reduced to less than 0.3, the best result is 0.16. Otherwise, in real experiments, 30 initial particle populations were used. The number of iterations and the optimization results show that when the number of iterations reaches 5, the optimization effect is significant, and the calculation amount is 150 calculation cycles. When the number of iterations reaches 10, the iteration results tend to be stable with an equivalent of 300 calculation cycles.

In addition, without parallel calculations, the total time for the non-optimized calculation is 4.1531 seconds, with sub-pixel edge positioning time of 0.7519 seconds. The calculation time for a single optimization cycle is 3.7301 seconds. The above results are all completed under the CPU (E3-1231 v3) and the platform (Matlab-2016). The parallel acceleration technology is not used in the calculation process.

The real calibration results of six sets are shown in Table. 3.

TABLE 3. The real experimental results.

Group Num.	1	2	3	4	5	6
f_y (pixel)	3935.98	3832.49	4015.54	3910.04	3922.13	3746.91
y_0 (pixel)	1369.76	1298.90	1431.94	1487.52	1411.91	1155.33
φ_1 (°)	1.8646	3.6266	2.3484	1.7958	3.4967	3.3025
φ_2 (°)	2.8042	2.8295	3.2826	2.2509	3.7729	3.7782
φ_3 (°)	-41.3611	-37.1145	-43.5491	-41.1422	-38.5364	35.4292
T_1 (mm)	-12.8825	-16.9780	-17.3401	-13.0101	-18.3598	-16.7858
T_2 (mm)	-65.9514	-34.2871	-64.9117	-64.6011	-48.2752	-17.0288
T_3 (mm)	467.9280	455.3200	468.0540	464.7990	466.3009	442.6813

VII. CONCLUSION

In this paper, a new calibration method of line camera is proposed. This method uses the space target method to carry on the static calibration, the line reference target pattern such as the conventional space parallel line group or the parallel block is changed. The method of point reference calibration based on the space rings group is constructed. After computer simulation and real experimental data, the effectiveness of the method is verified. Compared with dynamic scanning and other methods, the proposed method has strong operability and portability.

REFERENCES

[1] Z. Zhang, "A flexible new technique for camera calibration," *IEEE Trans. Pattern Anal. Mach. Intell.*, vol. 22, no. 11, pp. 1330–1334, Nov. 2000.
[2] X. Meng and Z. Hu, "A new easy camera calibration technique based on circular points," *Pattern Recognit.*, vol. 36, no. 5, pp. 1155–1164, May 2003.
[3] R. Horaud, R. Mohr, and B. Lorecki, "On single-scanline camera calibration," *IEEE Trans. Robot. Autom.*, vol. 9, no. 1, pp. 71–75, Feb. 1993.
[4] J. Draréni, S. Roy, and P. Sturm, "Plane-based calibration for linear cameras," *Int. J. Comput. Vis.*, vol. 91, no. 2, pp. 146–156, 2011.
[5] B. Hui, G. Wen, Z. Zhao, and D. Li, "Line-scan camera calibration in close-range photogrammetry," *Opt. Eng.*, vol. 51, no. 5, p. 053602, 2012.
[6] B. Hui, J. Zhong, G. Wen, and D. Li, "Determination of line scan camera parameters via the direct linear transformation," *Opt. Eng.*, vol. 51, no. 11, p. 113201, 2012.
[7] B. Hui, G. Wen, P. Zhang, and D. Li, "A novel line scan camera calibration technique with an auxiliary frame camera," *IEEE Trans. Instrum. Meas.*, vol. 62, no. 9, pp. 2567–2575, Sep. 2013.
[8] B. Sun, J. Zhu, L. Yang, S. Yang, and Z. Niu, "Calibration of line-scan cameras for precision measurement," *Appl. Opt.*, vol. 55, no. 25, pp. 6836–6843, 2016.
[9] B. Sun, J. Zhu, L. Yang, S. Yang, and Y. Guo, "Sensor for in-motion continuous 3D shape measurement based on dual line-scan cameras," *Sensors*, vol. 16, no. 11, p. 1949, 2016.
[10] B. Sun, J. Zhu, L. Yang, Y. Guo, and J. Lin, "Stereo line-scan sensor calibration for 3D shape measurement," *Appl Opt.*, vol. 56, no. 28, pp. 7905–7914, 2017.
[11] C. A. Luna, M. Mazo, J. L. Lazaro, and J. F. Vazquez, "Calibration of line-scan cameras," *IEEE Trans. Instrum. Meas.*, vol. 59, no. 8, pp. 2185–2190, Aug. 2010.
[12] E. Lilienblum, A. Al-Hamadi, and B. Michaelis, "A coded 3D calibration method for line-scan cameras," in *Proc. German Conf. Pattern Recognit. (GCPR)*, 2013, pp. 81–90.
[13] E. Lilienblum and A. Al-Hamadi, "A structured light approach for 3-D surface reconstruction with a stereo line-scan system," *IEEE Trans. Instrum. Meas.*, vol. 64, no. 5, pp. 1258–1266, May 2015.
[14] D. Li, G. Wen, B. W. Hui, S. Qiu, and W. Wang, "Cross-ratio invariant based line scan camera geometric calibration with static linear data," *Opt. Laser Eng.*, vol. 62, pp. 119–125, Nov. 2014.

[15] S. Ghosal and R. Mehrotra, "Orthogonal moment operators for subpixel edge detection," *Pattern Recognit.*, vol. 26, no. 2, pp. 295–306, 1993.
[16] F. Bouchara, "Efficient algorithm for computation of the second-order moment of the subpixel-edge position," *Appl. Opt.*, vol. 43, no. 23, pp. 4550–4558, 2004.
[17] R. Archibald, J. Gelb, and A. Yoon, "Polynomial fitting for edge detection in irregularly sampled signals and images," *SIAM J. Numer. Anal.*, vol. 43, no. 1, pp. 259–279, 2005.
[18] R. M. Haralick, "Digital step edges from zero crossing of second directional derivatives," *IEEE Trans. Pattern Anal. Mach. Intell.*, vol. PAMI-6, no. 1, pp. 58–68, Jan. 1984.
[19] T. Aydin, Y. Yemez, E. Anarim, and B. Sankur, "Multidirectional and multiscale edge detection via M-band wavelet transform," *IEEE Trans. Image Process.*, vol. 5, no. 9, pp. 1370–1377, Sep. 1996.
[20] H. Zunfeng, D. Hongshe, and L. Xiaorui, "A novel fast subpixel edge location method based ON Sobel-OFMM," in *Proc. IEEE, Int. Conf. Autom. Logistics*, Sep. 2008, pp. 828–832.
[21] A. Trujillo-Pino, K. Krissian, M. Alemán-Flores, and D. Santana-Cedrés, "Accurate subpixel edge location based on partial area effect," *Image Vis. Comput.*, vol. 31, no. 1, pp. 72–90, 2013.
[22] K. Dabov, A. Foi, V. Katkovnik, and K. Egiazarian, "Image denoising with block-matching and 3D filtering," *Proc. SPIE*, vol. 064, p. 606414, Feb. 2006.
[23] L.-L. Tang, Q.-C. Zhang, and S. Hu, "An improved algorithm for canny edge detection with adaptive threshold," *Opto-Electron. Eng.*, vol. 38, pp. 127–132, 2011.
[24] D. C. Brown, "Close-range camera calibration," *Photogramm. Eng.*, vol. 37, no. 8, pp. 855–866, 1971.
[25] O. Faugeras, *Three-Dimensional Computer Vision: A Geometric Viewpoint*. MIT, 1993, pp. 51–66.
[26] J. Kennedy and R. Eberhart, "A new optimizer using particle swarm theory," in *Proc. 6th Int. Symp. IEEE Micro Mach. Human Sci.*, Oct. 1995, pp. 39–43.

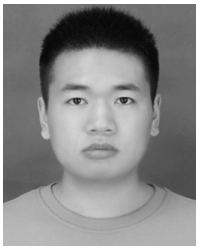

MENGHUI NIU received the B.E. degree from the School of Henan University of Science and Technology, Luoyang, China, in 2013, and the M.S. degree from the School of Mechanical Engineering and Automation, Northeastern University, Shenyang, China, in 2016, where he is currently pursuing the Ph.D. degree. His research interests include machine vision and image processing.

KECHEN SONG received the B.S., M.S., and Ph.D. degrees from the School of Mechanical Engineering and Automation, Northeastern University, Shenyang, China, in 2009, 2011, and 2014, respectively. He has been a Teacher with Northeastern University, China, since 2014. His research interests include vision-based inspection system for steel surface defects, surface topography, image processing, and pattern recognition.

XIN WEN received the B.E. and M.S. degrees from the School of Mechanical Engineering, Liaoning Shihua University, Fushun, China, in 2012 and 2015, respectively. She is currently pursuing the Ph.D. degree with the School of Mechanical Engineering and Automation, Northeastern University, Shenyang, China. Her research interests include surface topography and machine vision.

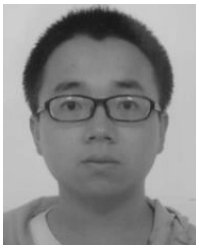

DEFU ZHANG received the B.E. degree from the School of Mechanical Design, Manufacturing and Automation, Hebei University, Baoding, China, in 2014, and the M.S. degree from the School of Mechanical Engineering and Automation, Northeastern University, Shenyang, China, as joint training of students with the Shenyang Institute of Automation, Chinese Academy of Sciences, in 2017. He is currently pursuing the Ph.D. degree with the School of Mechanical Engineering and Automation, Northeastern University. His research interests include machine vision and salient object detection.

YUNHUI YAN received the B.S., M.S., and Ph.D. degrees from the School of Mechanical Engineering and Automation, Northeastern University, Shenyang, China, in 1981, 1985, and 1997, respectively. He has been a Teacher with Northeastern University, China, since 1982, and became a Professor in 1997. From 1993 to 1994, he was with the Tohoku National Industrial Research Institute as a Visiting Scholar. His research interests include intelligent inspection, image processing, and pattern recognition.